

# Estimating Mechanical Properties of the Heart Using Dynamic Modeling and Magnetic Resonance Imaging

Aleksandar Jeremić and Arye Nehorai†§

† EECS Department (M/C 154), The University of Illinois at Chicago, 851 S. Morgan Street, Chicago, Illinois 60607-7053, USA

E-mail: [ajeremic@ece.uic.edu](mailto:ajeremic@ece.uic.edu) and [nehorai@ece.uic.edu](mailto:nehorai@ece.uic.edu)

**Abstract.** We present a method for estimating mechanical properties, active stress and passive elasticity modulus, of the *in vivo* heart using 2D magnetic resonance imaging (MRI) tissue-tagging and intra-ventricular pressure measurements. It has been shown that alterations in these properties may pre-date the onset of certain cardiac dysfunctions. We assume that the myocardium's stiffness tensor is non-homogeneous and propose to model this non-homogeneity using a set of *a priori* known basis functions and unknown coefficients. We combine this globally defined physical model with a finite-element formulation and dynamic analysis, and apply non-linear least squares to obtain the unknown parameters (basis functions coefficients.) We evaluate the performance of the proposed estimator by computing the confidence region for the estimated parameters. Numerical examples demonstrate the applicability of our results.

## 1. Introduction

Development of *in vivo* techniques for the quantifying regional myocardial mechanical properties is important to both academic and clinical research. From an academic standpoint, the development of such techniques enables the testing of fundamental constitutive models of the intact, *in vivo* heart. This may provide insights into regional ventricular function in patients with heart disease. The effects of pathological cardiac conditions on the mechanical properties of the heart are only vaguely known. Complicating the matter is the fact that most pathological conditions leading to heart disease affect the heart locally (regionally). Regional properties of the cardiac muscle can be measured only by *in vitro* uniaxial or biaxial tests performed on isolated muscles or strips of ventricular myocardium. The clinician however, is currently able to assess *in vivo* ventricular function of the heart only on a global level (e.g. stroke volume) or on a limited regional level (e.g., echocardiography).

A great deal of effort has been placed on the development of forward mathematical models in which the deformation is deduced starting from the active stress generated during contraction and assuming known mechanical properties of the heart. Complementary to this approach is the determination of the aforementioned regional mechanical properties of myocardial tissue from observed deformation. This approach is usually referred to as the inverse problem. Estimated inverse models may provide opportunities to explore the regional ventricular functions and their relation to the heart's function on a global level more fully.

In clinical research, *in vivo* inverse techniques may be useful to develop measures of ventricular function for detecting cardiac disease. Since heart disease is the leading cause of death in United States, it has been the subject of great interest in clinical cardiovascular physiology and pathophysiology research. As a result, numerous invasive and non-invasive diagnostic techniques that measure "abnormal" ventricular functions to detect cardiac disease are in use today. Whereas varying degrees of success have been achieved in detecting advanced disease, relatively poor results have been obtained for patients with early disease. Since alterations in the mechanical properties may pre-date the onset [1], [2] of cardiac dysfunction, an inverse solution can be potentially useful for detecting a cardiac disease in an early stage with sufficient sensitivity.

Historically, *in vivo* determination of the heart's mechanical properties has been determined by pressure-volume studies employing relatively simple mathematical models [3], [4]. This approach, while useful for estimating the ventricle's global characteristics, is unsuitable for understanding regional variations in the heart's material properties or the anisotropy of cardiac muscle. To fully characterize the complexities of the myocardial mechanical properties, an approach based on the theory of elasticity [5] is required. Recent advances in magnetic resonance imaging (MRI) and finite-element (FE) methods were used to estimate the mechanical properties, *in vivo* in the passive part of the heart cycle (diastole) [6].

We present a method for determining both active and passive mechanical properties of the myocardium using two-dimensional (2D) short-axis tagged MR images and intra-ventricular pressure measurements. Tissue-tagging MR imaging technique (see e.g. [7]) permits characterization of the deformative behavior of intra-myocardial tissue. Radio-frequency (RF) pulses are used to set up a grid of tag lines whose motions (systolic contraction and diastolic expansion) are tracked throughout the cardiac cycle. We model the heart motion using small-strain dynamic analysis, based on continuum mechanics theory, and assume that the myocardium is heterogeneous, anisotropic and non-linear hyper-elastic material. To account for regional variations (heterogeneity), we model the stiffness related mechanical parameters of the heart using a set of *a priori* known basis functions and unknown coefficients. By applying time-dependent FE analysis to the resulting equation, we introduce a 2D dynamic model that relates displacements of the tag points at various locations (in the cross-sectional plane) during the heart cycle to the mechanical parameters and ventricular pressure. To compute the displacement field we use an automated algorithm to detect the tag points, i.e. intersections of individual pairs of tag lines. We combine a finite-element formulation with dynamic modeling to determine the predicted pressure and then estimate the mechanical parameters by minimizing the distance measure between the predicted pressure and pressure measurements using non-linear optimization of the distance measure.

The structure of this paper is as follows: in Section 2, we describe the physical model; we assume that the material's stiffness tensor, defining the stress-strain relations, is anisotropic and non-homogeneous. We model the heart-wall motion using the virtual displacement principle resulting in a non-linear equation for the incremental displacements. In Section 3, we derive a finite-element approximation of the physical model and transform it to a form amenable to analysis by statistical signal processing techniques. In Section 4, we describe our measurement model (based on tagged MR images and pressure measurements) and techniques for estimating the unknown coefficients in the model using a non-linear optimization of the error between the model-predicted and measured pressures. In order to encapsulate the non-homogeneity of the stress-strain tensor and contractile stress, we introduce our basis functions model for the mechanical properties (active and passive) of the heart. In Section 5, we illustrate the applicability of our method through numerical examples. In Section 6, we discuss our results and future research.

## 2. Mechanical Model of the Heart

In this section, we describe the heart's geometry, myocardium structure, and corresponding mathematical (forward) models that will be used later in the paper for solving the inverse problem. From the perspective of engineering mechanics, the cardiac muscle should be considered as an inhomogeneous, anisotropic, and incompressible material. However, recent reports indicate that the incompressibility of the heart is questionable [8] at least because the phasic nature (active and passive phase) of arterial and venous coronary flow indicates that intra-coronary blood volume varies in time. Moreover, in the present study, we analyze only the motion of 2D cross-sectional models in which the incompressibility assumption (constant cross-sectional area) is unrealistic. Therefore, we shall assume that the cross-sectional cardiac tissue is compressible.

### 2.1. Physical Model

The mechanical behavior of a hyper-elastic body such as the myocardium is fully described by the deformation, the corresponding internal elastic forces and external forces.

In analyzing the deformation of the heart's cross-section we assume that the heart's motion is non-rigid so that particles of the body cannot move without deformation. Since the deformation of the cross-section is rather complex, we use the most general approach in defining the deformation measure. We first assert that the deformation can be measured only relatively, with respect to some reference state in which the cross-sectional plane is undeformed. Following the approach of [15] we use the end-of-diastole state as the reference state. In principle, at a reference state the heartwall should be undeformed so that the mechanical properties estimates for different subjects and/or corresponding to different times can be compared. However in practice different heartwalls at the end-of-diastole may be at different level of "residual" deformation. We will discuss later how the proposed techniques can be modified to account for the residual deformation.

Consider a material point  $P$  in the cross-sectional plane and let  $\mathbf{r}(t)$  be the location of  $P$  at time  $t$ . Then the displacement vector associated with that point is  $\mathbf{r}(t) - \mathbf{r}_0$  where  $\mathbf{r}_0$  is the location of  $P$  at the reference state. The displacement field of the heart's cross-section at time  $t$  is given by  $\mathbf{u}(\mathbf{r}, t)$  which corresponds to the displacement of a material point located at  $\mathbf{r}$  at time  $t$ . The discretized displacement field can be measured from tagged MR images.

To describe the deformation of the heart, we use the Eulerian definition of strain measure [5]

$$\begin{aligned}\epsilon_{xx}(\mathbf{r}, t) &= \frac{\partial u_x(\mathbf{r}, t)}{\partial x} \\ \epsilon_{yy}(\mathbf{r}, t) &= \frac{\partial u_y(\mathbf{r}, t)}{\partial y} \\ \epsilon_{xy}(\mathbf{r}, t) &= \frac{1}{2} \left( \frac{\partial u_y(\mathbf{r}, t)}{\partial x} + \frac{\partial u_x(\mathbf{r}, t)}{\partial y} \right)\end{aligned}\quad (1)$$

where  $\epsilon_{xx}(\mathbf{r}, t)$  and  $\epsilon_{yy}(\mathbf{r}, t)$  are the elongations in the  $x$  and  $y$  directions,  $\epsilon_{xy}(\mathbf{r}, t)$  is the shear strain, and  $u_x(\mathbf{r}, t)$  and  $u_y(\mathbf{r}, t)$  are the displacements in the  $x$  and  $y$  directions respectively i.e.  $\mathbf{u}(\mathbf{r}, t) = [u_x(\mathbf{r}, t), u_y(\mathbf{r}, t)]^T$ . Since the deformation at any point is completely described by the elongations and shear strain, we will use the strain vector

$$\boldsymbol{\epsilon}(\mathbf{r}, t) = [\epsilon_{xx}(\mathbf{r}, t), \epsilon_{yy}(\mathbf{r}, t), \epsilon_{xy}(\mathbf{r}, t)]^T \quad (2)$$

as a deformation measure.

The deformation of the cross-sectional plane is caused by external forces, electro-mechanical (due to the propagation of an electric pulse) and boundary tractions (due to the intra-ventricular pressures). In response to the action of the external forces, internal forces are produced between the parts of the cross-sectional plane. The magnitudes of such forces are usually defined by their intensity, i.e. the amount of force per unit area (or length in 2D problems). In analyzing internal forces, this intensity is called stress. Similar to the strain measure, the corresponding stress is described by a stress vector

$$\boldsymbol{\sigma}(\mathbf{r}, t) = [\sigma_{xx}(\mathbf{r}, t), \sigma_{yy}(\mathbf{r}, t), \sigma_{xy}(\mathbf{r}, t)]^T \quad (3)$$

where  $\sigma_{xx}(\mathbf{r}, t)$  and  $\sigma_{yy}(\mathbf{r}, t)$  are normal stresses and  $\sigma_{xy}(\mathbf{r}, t)$  is the shear stress.

We split the ventricular stress vector  $\boldsymbol{\sigma}(\mathbf{r}, t)$  into two parts: passive stress  $\boldsymbol{\sigma}^p(\mathbf{r}, t)$ , resulting from the deformation of the myocardial tissue, and active contractile stress  $\boldsymbol{\sigma}^a(\mathbf{r}, t)$ , resulting from the isometric contraction of the muscle fiber caused by a propagating electric pulse.

For a hyper-elastic body, such as the myocardium, the passive stress-strain relationship (the passive stress developed within a heart undergoing deformation) is determined by the strain energy function  $w(\mathbf{r}, \boldsymbol{\epsilon})$  which represents the strain

energy per unit volume or the work of external forces needed to achieve the deformation  $\boldsymbol{\epsilon}$ . The passive stress-strain relationship is then given by [5]

$$\boldsymbol{\sigma}^p(\mathbf{r}, t) = \frac{\partial w(\mathbf{r}, \boldsymbol{\epsilon}(\mathbf{r}, t))}{\partial \boldsymbol{\epsilon}(\mathbf{r}, t)}. \quad (4)$$

It has been shown [10] that the pseudo-strain energy function of the heart is approximated well by an exponential strain energy function. We use the pseudo-strain energy model [10]

$$w(\mathbf{r}, \boldsymbol{\epsilon}(\mathbf{r}, t)) = a \left\{ e^{[\boldsymbol{\epsilon}^T(\mathbf{r}, t) D(\mathbf{r}) \boldsymbol{\epsilon}(\mathbf{r}, t)]} - 1 \right\} \quad (5)$$

where  $a$  is the normal stiffness in units of  $\text{J}/\text{m}^3$ , and  $D(\mathbf{r})$  is a matrix of non-homogeneous stiffness related mechanical properties in units of  $\text{N}/\text{m}^2$ . To account for possible non-homogeneity of the myocardium we have introduced the spatial dependence of  $D(\mathbf{r})$ .  $D(\mathbf{r})$  is a  $3 \times 3$  symmetric matrix. Substituting (5) into (4) yields

$$\begin{aligned} \boldsymbol{\sigma}^p(\mathbf{r}, t) &= 2ae^{[\boldsymbol{\epsilon}^T(\mathbf{r}, t) D(\mathbf{r}) \boldsymbol{\epsilon}(\mathbf{r}, t)]} D(\mathbf{r}) \boldsymbol{\epsilon}(\mathbf{r}, t) \\ &= E(\mathbf{r}, t) \boldsymbol{\epsilon}(\mathbf{r}, t), \end{aligned} \quad (6)$$

where  $E(\mathbf{r}, t)$  is the stiffness matrix given by

$$E(\mathbf{r}, t) = 2ae^{[\boldsymbol{\epsilon}^T(\mathbf{r}, t) D(\mathbf{r}) \boldsymbol{\epsilon}(\mathbf{r}, t)]} D(\mathbf{r}). \quad (7)$$

For the active stress, we adopt the model from [16]. Accordingly

$$\begin{aligned} \boldsymbol{\sigma}_f^a(t) &= \frac{1}{2} \sigma_f^{\max} [1 - \cos \psi^a(t)] \mathbf{i}_f \\ &= \sigma_f^a(t) \mathbf{i}_f, \end{aligned} \quad (8)$$

where  $\boldsymbol{\sigma}_f^a(t)$  is the active stress vector in the fiber coordinates system,  $\mathbf{i}_f$  is the unit vector in the fiber direction,  $\sigma_f^{\max}$  is the maximum isometric tension value, and

$$\psi^a(t) = \begin{cases} \pi \frac{t-t_d}{t_0} & t_d < t < t_0 + t_d \\ -\pi \frac{t-t_0-t_r}{t_r} & t_d + t_0 \leq t < t_d + t_0 + t_r \\ 0 & \text{elsewhere,} \end{cases} \quad (9)$$

where  $t_d$  is the duration of diastole,  $t_0$  is the time to peak-tension (measure from the beginning of the systole), and  $t_r$  is the duration of cardiac muscle relaxation which, in general, is a function of strain given by the following relation [17]

$$t_r = b \sqrt{2 \|\boldsymbol{\epsilon}(\mathbf{r}, t)\|^2 + 1}, \quad (10)$$

where  $b$  is a constant in seconds.

The active stress  $\boldsymbol{\sigma}^a$ , in the cross-sectional plane, consists of two longitudinal components,  $\sigma_{xx}^a$  and  $\sigma_{yy}^a$ , as well as shear stress  $\sigma_{xy}^a$ . The components of the cross-sectional active stress are computed from (8)

$$\begin{aligned} \boldsymbol{\sigma}^a(\mathbf{r}, t) &= \sigma_f^a(t) \begin{bmatrix} \cos^2 \psi(\mathbf{r}) \cos^2 \theta \\ \cos^2 \psi(\mathbf{r}) \sin^2 \theta \\ \sin^2 \psi(\mathbf{r}) \cos \theta \sin \theta \end{bmatrix} \\ &= \sigma_f^a(t) \boldsymbol{\gamma}(\mathbf{r}), \end{aligned} \quad (11)$$

where  $\psi(\mathbf{r})$  is a fiber angle,  $\theta$  is the azimuth, and

$$\boldsymbol{\gamma}(\mathbf{r}) = [\cos^2 \psi(\mathbf{r}) \cos^2 \theta, \cos^2 \psi(\mathbf{r}) \sin^2 \theta, \sin^2 \psi(\mathbf{r}) \cos \theta \sin \theta]^T. \quad (12)$$

### 3. Heart Motion Equations

In this section we obtain the governing equations of the motion i.e. we obtain the displacement field for a given set of mechanical properties and boundary tractions (intra-ventricular pressures). This is often referred to as a forward problem.

We continue to consider the cross-sectional plane of the heart as an elastic body containing region of material with varying surface denoted by  $S(t)$ . The cross-sectional plane is loaded by intra-ventricular pressures along the boundary of  $S(t)$  which is in equilibrium with the stress. To formulate the aforementioned equations we use the principle of virtual work [5]. This principle requires that if a deformable body in equilibrium is subjected to arbitrary virtual displacements associated with a compatible deformation of the body, then the virtual work of the external forces is equal to the virtual strain energy of its internal stresses.

*The Equation of Elastodynamics in Two Dimensions*

At any time  $t$ , the equilibrium equations of the cross-sectional plane at any point are given by [5]

$$\mathcal{D}^T \boldsymbol{\sigma}(\mathbf{r}, t) = \rho \frac{\partial^2 \mathbf{u}(\mathbf{r}, t)}{\partial t^2}, \quad (13)$$

where

$$\mathcal{D} = \begin{bmatrix} \frac{\partial}{\partial x} & 0 \\ 0 & \frac{\partial}{\partial y} \\ \frac{\partial}{\partial x} & \frac{\partial}{\partial y} \end{bmatrix} \quad (14)$$

is a differential operator matrix and  $\rho$  is the mass density of the myocardium. The l.h.s. of equation (13) corresponds to the elastic forces and the r.h.s. corresponds to the inertial forces.

The boundary conditions of (13) are given in terms of the pressure vector defined as  $\mathbf{p}(\mathbf{r}, t) = p(t)\mathbf{n}(\mathbf{r}, t)$  where  $\mathbf{n}(\mathbf{r}, t)$  is the unit normal vector pointing outside of the myocardium and  $p(t)$  is the intra-ventricular pressure.

In the reference coordinate system, the pressure components  $p_x(\mathbf{r}, t)$  and  $p_y(\mathbf{r}, t)$  are related to the stress components through

$$\begin{aligned} p_x(\mathbf{r}, t) &= \sigma_{xx}(\mathbf{r}, t)\cos\alpha + \sigma_{xy}(\mathbf{r}, t)\sin\alpha, \\ p_y(\mathbf{r}, t) &= \sigma_{xy}(\mathbf{r}, t)\cos\alpha + \sigma_{yy}(\mathbf{r}, t)\sin\alpha, \end{aligned} \quad (15)$$

where  $\alpha$  is the angle measured from the positive  $x$  axis to  $\mathbf{n}(t)$ . However, it is more convenient to specify the normal and tangential components of the traction vector, denoted by  $\tau_n$  and  $\tau_t$  and are given by

$$\begin{aligned} p_n(\mathbf{r}, t) &= p_x(\mathbf{r}, t)\cos\alpha + p_y(\mathbf{r}, t)\sin\alpha, \\ p_t(\mathbf{r}, t) &= -p_x(\mathbf{r}, t)\sin\alpha + p_y(\mathbf{r}, t)\cos\alpha. \end{aligned} \quad (16)$$

Solution of a continuum mechanics problem requires the enforcement of constraints on rigid body translation and rotation. For the myocardium, selection of suitable constraints is problematic because such constraints may result in unphysiologic stress concentrations and consequently in unreasonable deformations. One of the principal boundary conditions substantially affecting the mechanical behavior of the heart is the pericardial pressure. Following the approach of [6] we use spring constraints to model this effect assuming that the epicardial edges are constrained by tractions proportional to the normal displacement

$$p_n(\mathbf{r}, t) = \kappa u_n(\mathbf{r}, t) \quad (17)$$

where  $p_n(\mathbf{r}, t)$  is the normal traction,  $u_n(\mathbf{r}, t)$  is the normal component of displacement and  $\kappa$  is a linear spring constant. Let  $l_{\text{epi}}(t)$  be the epicardial boundary of the heart's cross-section at time  $t$ . Similarly let  $l_{\text{len}}(t)$  and  $l_{\text{ren}}(t)$  denote the left-ventricular and right-ventricular endocardial boundaries. Using this notation, the boundary conditions are given by

$$\begin{aligned} p_n(\mathbf{r}, t) &= \begin{cases} p^{\text{LV}}(t) & \text{for } \mathbf{r} \in l_{\text{len}}(t) \\ p^{\text{RV}}(t) & \text{for } \mathbf{r} \in l_{\text{ren}}(t) \\ \kappa u_n(\mathbf{r}, t) & \text{for } \mathbf{r} \in l_{\text{epi}}(t) \end{cases} \\ p_t(\mathbf{r}, t) &= 0 \quad \text{for } \mathbf{r} \in l(t), \end{aligned} \quad (18)$$

where  $l(t)$  is the boundary of the cross-section consisting of the endocardial and epicardial boundary, and  $p^{\text{LV}}(t)$  and  $p^{\text{RV}}(t)$  are the left and right intra-ventricular pressures respectively.

#### The Principle of Virtual Displacements

We establish the relationship between the stresses and displacements using the principle of virtual work rather than directly applying Newton's laws of motion. In particular we apply the principle of virtual displacements in which we deal with the true forces and virtual displacements.

Consider the cross-sectional plane of the heart at time  $t$  which is under the action of internal and external forces. Now imagine that the cross-sectional plane undergoes completely arbitrary virtual displacement  $\delta\mathbf{v}$  during which all the forces remain acting in their original directions. We use the symbol  $\delta\mathbf{v}$  merely to point that it is a virtual displacement and has nothing to do (for the present) with any true displacement which defines the true motion of the plane. The principle of virtual displacement requires that the work of internal forces  $w_I(\mathbf{u}, \delta\mathbf{v}, t)$ , related to the elastic properties of myocardium, equals the work of external forces  $w_E(\mathbf{u}, \delta\mathbf{v}, t)$ , related to inertial forces and boundary traction, i.e.

$$w_I(\mathbf{u}, \delta\mathbf{v}, t) = w_E(\mathbf{u}, \delta\mathbf{v}, t) \quad (19)$$

Next, we compute  $w_I(\mathbf{u}, \delta\mathbf{v}, t)$  using [5]

$$w_I(\mathbf{u}, \delta\mathbf{v}, t) = \int_{S(t)} (\mathcal{D}\delta\mathbf{v})^T \boldsymbol{\sigma}(\mathbf{r}, t) d\mathbf{r}. \quad (20)$$

Then, using (6) and (8) we can rewrite (20) as

$$w_I(\mathbf{u}, \delta\mathbf{v}, t) = \int_{S(t)} (\mathcal{D}\delta\mathbf{v})^T E(\mathbf{r}, t) \mathcal{D}\mathbf{u}(\mathbf{r}, t) d\mathbf{r} + \int_{S(t)} \sigma_f^a(t) (\mathcal{D}\delta\mathbf{v})^T \boldsymbol{\gamma}(\mathbf{r}) d\mathbf{r}. \quad (21)$$

Similarly, for  $w_E(\mathbf{u}, \delta\mathbf{v}, t)$  we have

$$\begin{aligned} w_E(\mathbf{u}, \delta\mathbf{v}, t) = & \int_{l_{\text{epi}}(t)} \kappa (\mathcal{D}\delta\mathbf{v})^T \mathbf{n}_{\text{epi}}(\mathbf{r}, t) \mathbf{n}_{\text{epi}}^T(\mathbf{r}, t) \mathbf{u}(\mathbf{r}, t) dl + \int_{S(t)} \rho(\delta\mathbf{v})^T \frac{\partial^2 \mathbf{u}(\mathbf{r}, t)}{\partial t^2} d\mathbf{r} + \\ & + \int_{l_{\text{ren}}(t)} p^{\text{RV}}(t) (\mathcal{D}\delta\mathbf{v})^T \mathbf{n}_{\text{ren}}(\mathbf{r}, t) dl + \int_{l_{\text{len}}(t)} p^{\text{LV}}(t) (\mathcal{D}\delta\mathbf{v})^T \mathbf{n}_{\text{len}}(\mathbf{r}, t) dl + \end{aligned} \quad (22)$$

where the first term on the r.h.s. side is the work of inertial force, the second term is the work of the force cause by left-ventricular pressure, the third term is the work of the elastic forces acting on the pericardial boundary, and the last term is the work of the cause by right-ventricular pressure.

#### 4. Finite-Element Solution

The governing equation of motion (19) cannot be solved analytically due to the non-linear stress-strain relationship and non-trivial geometrical shape of the cross section, also (19) has to be satisfied *for all*  $\delta\mathbf{v}$ . Since we cannot work with infinitely many functions it is necessary to recast the problem in purely algebraic form, involving only the basic arithmetic operations. To achieve this goal we will use a finite-element (FE) method which is a standard technique for discretizing equations corresponding to continuum problems. The FE method is a natural choice since in our problem we deal with the spatially discretized displacement field  $\mathbf{u}$  which can be measured only at tag points. Therefore, our rationale behind this approach is to replace the infinite set of numbers representing a solution  $\mathbf{u}$  by a finite number of unknown variables corresponding to the displacement of tag points..

##### 4.1. Finite-Element Concept

We wish to approximate the displacement function  $\mathbf{u}$  in the heart's cross-section  $S(t)$  by dividing it into a number of non-overlapping subdomains or elements  $S^k(t)$  and then constructing an approximation in a piecewise manner over each sub-domain

$$\hat{\mathbf{u}}^k(\mathbf{r}, t) = \sum_{i=1}^{n_k} \mathbf{a}_i^k(t) \phi_i^k(\mathbf{r}, t) \quad \text{for } \mathbf{r} \in S^k(t), \quad (23)$$

where  $\mathbf{a}_i^k(t)$  are the vectors of coefficients and  $\phi_i^k(\mathbf{r}, t)$  are *a priori* known basis functions used to approximate  $\mathbf{u}$  over the  $k$ th element, see [18]. It can be shown that by using  $p$ -version of finite element method (see [19]) the displacement function over  $k$ -th sub-domain can be written as

$$\hat{\mathbf{u}}^k(\mathbf{r}, t) = \Phi^k(\mathbf{r}, t) \mathbf{d}^k(t), \quad (24)$$

where  $\Phi^k(\mathbf{r}, t)$  is the interpolation matrix for  $k$ -th subdomain at time  $t$  and  $\mathbf{d}^k(t)$  is the nodal displacement vector at time  $t$ . Therefore, equation (24) provides the discrete approximation of the displacement field for a single element. Observe that  $\hat{\mathbf{u}}^k(\mathbf{r}, t)$  corresponds to the displacement defined over the standard element and thus must be mapped to a "real" element using mapping functions.

We wish to determine the displacement function  $\mathbf{u}$  so that equation (19) is satisfied for all  $\delta\mathbf{v}$ . Let  $\mathbf{r}_i(t)$  be the location of the  $i$ th tag point at time  $t$  and  $\mathbf{r}_i(0)$  be its location at the reference state,  $i = 1, \dots, m$  where  $m$  is the number of tag points. Then the displacement of tag points at time  $t$  is given by

$$\mathbf{d}_u(t) = [(\mathbf{r}_1(t) - \mathbf{r}_1(0))^T, (\mathbf{r}_2(t) - \mathbf{r}_2(0))^T, \dots, (\mathbf{r}_m(t) - \mathbf{r}_m(0))^T], \quad (25)$$

where we use subscript  $u$  to denote that the nodal displacement corresponds to the displacement field  $\mathbf{u}(\mathbf{r}, t)$ .

Using (24) any displacement function  $\mathbf{u}(\mathbf{r}, t)$  can be approximated with

$$\hat{\mathbf{u}}(\mathbf{r}, t) = \Phi(\mathbf{r}, t) \mathbf{d}_u(t), \quad (26)$$

where  $\Phi(\mathbf{r}, t)$  is the interpolation matrix chosen so that the approximation is exact at the tag points. Similarly, the virtual displacement can be represented as

$$\delta\mathbf{v} = \Phi(\mathbf{r}, t) \mathbf{d}_{\delta\mathbf{v}}, \quad (27)$$

where  $\mathbf{d}_{\delta\mathbf{v}}$  is the vector of arbitrary amplitudes.

Substituting (26) and (27) into (19) we have for the l.h.s. of (19)

$$\int_{S(t)} (\mathcal{D}\Phi(\mathbf{r}, t) \mathbf{d}_{\delta v})^T E(\mathbf{r}, t) (\mathcal{D}\Phi(\mathbf{r}, t) \mathbf{d}_u(t)) d\mathbf{r}, \quad (28)$$

and similarly, substituting  $v_n = (\delta \mathbf{v})^T \mathbf{n}(\mathbf{r}, t)$  for r.h.s. of (19)

$$\begin{aligned} & \int_{S(t)} \rho \mathbf{d}_{\delta v}^T \Phi^T(\mathbf{r}, t) \Phi(\mathbf{r}, t) \frac{\partial^2 \mathbf{d}_u(t)}{\partial t^2} d\mathbf{r} + \int_{l_{\text{epi}}(t)} \kappa \mathbf{d}_{\delta v}^T \Phi^T(\mathbf{r}, t) \mathbf{n}_{\text{epi}}(\mathbf{r}, t) \mathbf{n}_{\text{epi}}^T(\mathbf{r}, t) \Phi(\mathbf{r}, t) \mathbf{d}_u(t) dl + \\ & + \int_{l_{\text{len}}(t)} p^{\text{LV}}(t) \mathbf{d}_{\delta v}^T \Phi^T(\mathbf{r}, t) \mathbf{n}_{\text{len}}(\mathbf{r}, t) dl + \int_{l_{\text{ren}}(t)} p^{\text{RV}}(t) \mathbf{d}_{\delta v}^T \Phi^T(\mathbf{r}, t) \mathbf{n}_{\text{ren}}(\mathbf{r}, t) dl. \end{aligned} \quad (29)$$

Observe that equations (28) and (29) are the discrete version of the virtual principle equation (19).

Next, we define the global stiffness matrix (or the assembled stiffness matrix)

$$K(t) = \int_{S(t)} (\mathcal{D}\Phi(\mathbf{r}, t))^T E(\mathbf{r}, t) (\mathcal{D}\Phi(\mathbf{r}, t)) d\mathbf{r} + \int_{l_{\text{epi}}(t)} \kappa \Phi^T(\mathbf{r}, t) \mathbf{n}_{\text{epi}}(\mathbf{r}, t) \mathbf{n}_{\text{epi}}^T(\mathbf{r}, t) \Phi(\mathbf{r}, t) \mathbf{d}_u(t) dl, \quad (30)$$

the mass matrix

$$M(t) = \int_{S(t)} \rho \Phi^T(\mathbf{r}, t) \Phi(\mathbf{r}, t) d\mathbf{r}, \quad (31)$$

and load vector, corresponding to the total force acting on the boundary of the heart's cross-section,

$$\mathbf{f}(t) = \int_{l_{\text{len}}(t)} p^{\text{LV}}(t) \Phi^T(\mathbf{r}, t) \mathbf{n}_{\text{len}}(\mathbf{r}, t) dl + \int_{l_{\text{ren}}(t)} p^{\text{RV}}(t) \Phi^T(\mathbf{r}, t) \mathbf{n}_{\text{ren}}(\mathbf{r}, t) dl. \quad (32)$$

With this notation, the FE model becomes

$$\mathbf{d}_{\delta v}^T \left[ M(t) \frac{\partial^2 \mathbf{d}_u(t)}{\partial t^2} + K(t) \mathbf{d}_u(t) - \mathbf{f}(t) \right] = 0 \quad (33)$$

for all  $\mathbf{d}_{\delta v}$ . This condition is satisfied only when

$$M(t) \frac{\partial^2 \mathbf{d}_u(t)}{\partial t^2} + K(t) \mathbf{d}_u(t) = \mathbf{f}(t). \quad (34)$$

The elements of the global stiffness matrix  $K$  are computed as

$$K_{i,j}(t) = \int_{l_{\text{per}}(t)} \kappa \Phi_i^T(\mathbf{r}, t) \mathbf{n}_{\text{per}}(\mathbf{r}, t) \mathbf{n}_{\text{per}}^T(\mathbf{r}, t) \Phi_j(\mathbf{r}, t) \mathbf{d}_u(t) dl + \int_{S(t)} (\mathcal{D}\Phi_i(\mathbf{r}, t))^T E(\mathbf{r}, t) (\mathcal{D}\Phi_j(\mathbf{r}, t)) d\mathbf{r} \quad (35)$$

where  $\Phi_i$  is the  $i$ th column of  $\Phi$ . Observe that all  $\Phi_i$  are nonzero only over individual finite elements or adjacent finite elements. Similarly, the elements of the mass matrix are given by

$$M_{i,j}(t) = \int_{S(t)} \rho \Phi_i^T(\mathbf{r}, t) \Phi_j(\mathbf{r}, t) d\mathbf{r}. \quad (36)$$

The elements of global load vector  $\mathbf{f}(t)$ , are given by

$$\mathbf{f}_i(t) = \int_{l_{\text{len}}(t)} p_{\text{LV}}(t) \Phi_i^T(\mathbf{r}, t) \mathbf{n}_{\text{len}}(\mathbf{r}, t) dl + \int_{l_{\text{ren}}(t)} p_{\text{RV}}(t) \Phi_i^T(\mathbf{r}, t) \mathbf{n}_{\text{ren}}(\mathbf{r}, t) dl. \quad (37)$$

## 5. Parameter Estimation

In this section we derive a parametric statistical model using equation (34) in terms of the mechanical properties. We then describe estimation techniques for finding these properties using measurements of intra-ventricular pressure and tagged MR images. We evaluate the performance of the proposed techniques by computing confidence regions for the estimated parameters.

### 5.1. Model Development

We will use the term *passive properties* when referring to the mechanical properties that determine the passive stress (6) for a particular strain  $\epsilon$ . Similarly we will use the term *active properties* to denote mechanical properties that determine the active stress (8).

From (6) it follows that the passive stress is completely determined by the strain  $\epsilon$ , matrix  $D(\mathbf{r})$ , and normalized stiffness  $a$ . Since we wish to estimate the mechanical properties of the heart regionally, we consider heart as a non-homogeneous object by allowing spatial variations in the stiffness matrix  $D(\mathbf{r})$ . There are several ways in which one could model this type of non-homogeneity. The commonly used approach uses the model

$$D(\mathbf{r}) = \sum_{k=1}^{n_{e1}} D_k \phi^k(\mathbf{r})$$

$$\phi^k(\mathbf{r}) = \begin{cases} 1 & \mathbf{r} \in S^k \\ 0 & \text{elsewhere} \end{cases} \quad (38)$$

where  $S^k$  denotes the area of  $k$ th element. In this case the accuracy of the non-homogeneous modeling is determined by the size of the elements. We propose to model the non-homogeneity using a linear combination of an *a priori* known set of basis functions with unknown coefficients. Then, the  $(i, j)$ th entry of  $D(\mathbf{r})$  is given by

$$D_{i,j}(\mathbf{r}) = \sum_k^{n_{bp}} c_k^{i,j} \phi_k^{i,j}(\mathbf{r}), \quad (39)$$

where  $\{\phi_k^{i,j}(\mathbf{r})\}$  is the set of basis functions,  $n_{bp}$  is the number of basis functions for modeling the passive properties, and  $c_k^{i,j}$  are the coefficients where  $i, j = 1, 2, 3$  and  $k = 1, \dots, n_{bp}$ . Let  $\mathbf{c}_{i,j} = [c_1^{i,j}, \dots, c_{n_{bp}}^{i,j}]^T$ . Then we define the passive parameters vector  $\boldsymbol{\theta}_p = [a, \mathbf{c}_{1,1}^T, \mathbf{c}_{1,2}^T, \mathbf{c}_{1,3}^T, \mathbf{c}_{2,2}^T, \mathbf{c}_{2,3}^T, \mathbf{c}_{3,3}^T]^T$ .

We now define the active parameters. In order to encapsulate the spatio-temporal dependence of the active contraction (11), we use the following model

$$\boldsymbol{\sigma}^a(\mathbf{r}, t) = \sum_{i=1}^{n_{bas}} \mathbf{c}_i^g \phi_i^g(\mathbf{r}) \sum_{j=1}^{n_{bat}} c_j^\sigma \phi_j^\sigma(t), \quad (40)$$

where  $\{\phi_i^g(\mathbf{r})\}$  is the set of basis functions that models the spatial dependence of  $\mathbf{g}(\mathbf{r})$ ,  $n_{bas}$  and  $n_{bat}$  are the number of basis functions for modeling the spatial and temporal dependence of the active stress respectively, and  $\{\mathbf{c}_i^g\}$  are the unknown coefficient vectors. Similarly,  $\{\phi_j^\sigma(t)\}$  is the set of basis functions that models the temporal dependence of the active stress. We define the active parameters vector  $\boldsymbol{\theta}_a = [c_1^{gT}, \dots, c_{n_{bas}}^{gT}, c_1^\sigma, \dots, c_{n_{bat}}^\sigma]^T$ .

The number of unknown parameters in the models (39) and (40) is proportional to the number of basis functions. Furthermore, the number of active parameters is given by  $3n_b^2$  which may result in an ill-posed problem if  $n_b$  is large. In order to reduce the dimensionality of the estimation problem we need to exploit some *a priori* given information about the mechanical properties.

In the previous discussion we have not imposed any constraints on the structure of the stiffness related matrix  $D(\mathbf{r})$ . However,  $D(\mathbf{r})$  must be symmetric positive definite and moreover in 2D plane-strain analysis the entries  $D_{1,3}(\mathbf{r})$  and  $D_{2,3}(\mathbf{r})$  have to be zero for all  $\mathbf{r}$ , see [5]. Thus, the following conditions have to be satisfied

$$\begin{aligned} D_{1,1}(\mathbf{r}) &> 0, \\ D_{1,1}(\mathbf{r})D_{2,2}(\mathbf{r}) - D_{1,2}^2(\mathbf{r}) &> 0, \\ D_{3,3}(\mathbf{r}) &> 0, \end{aligned} \quad (41)$$

for all  $\mathbf{r}$ .

In order to further decrease the complexity of the problem we will assume that the myocardium is an isotropic material. In that case the entries of  $D(\mathbf{r})$  are given by [5]

$$\begin{aligned} D_{11}(\mathbf{r}) &= \frac{e(\mathbf{r})}{1 - \epsilon}, \\ D_{22}(\mathbf{r}) &= \frac{e(\mathbf{r})}{1 - \epsilon}, \\ D_{12}(\mathbf{r}) &= \frac{e(\mathbf{r})\epsilon}{1 - \epsilon}, \\ D_{33}(\mathbf{r}) &= \frac{e(\mathbf{r})}{1 + 2\epsilon}, \end{aligned} \quad (42)$$

where  $e(\mathbf{r})$  is the elasticity modulus and  $\varepsilon$  is the Poisson ratio. We model the non-homogeneity of the elasticity modulus using

$$e(\mathbf{r}) = \sum_{i=1}^{n_{be}} c_i^e \phi_i(\mathbf{r}) \quad (43)$$

where  $\{\phi_i(\mathbf{r})\}$  is the set of *a priori* known basis functions and  $\{c_i^e\}$  are the corresponding coefficients. Using this model the passive parameters vector becomes  $\boldsymbol{\theta}_p = [a, c_1^e, \dots, c_{n_{be}}^e]^T$  which has dimension  $n_{be} + 2$ . Moreover, the cumbersome anisotropic conditions (41) transform into

$$\begin{aligned} 0 < e(\mathbf{r}) \\ 0 < \varepsilon \leq 0.5. \end{aligned} \quad (44)$$

Next, we introduce the basis-functions model for the elasticity modulus

$$e(\mathbf{r}) = \sum_{i=1}^{n_{bp}} c_{e,i} \phi_{e,i}(\mathbf{r}), \quad (45)$$

where  $\phi_{e,i}(\mathbf{r})$  is the set of basis functions for modeling the elasticity modulus and  $c_{e,i}$  are the unknown coefficients. Then, to satisfy  $e(\mathbf{r}) > 0$  we first observe that

$$\min[e(\mathbf{r})] = \min \left[ \sum_{i=1}^{n_{bp}} c_{e,i} \phi_{e,i}(\mathbf{r}) \right] \geq \sum_{i=1}^{n_{bp}} c_{e,i} \min \phi_{e,i}(\mathbf{r}). \quad (46)$$

Therefore, the condition  $e(\mathbf{r}) > 0$  is satisfied for

$$\sum_{i=1}^{n_{bp}} c_{e,i} \min[\phi_{e,i}(\mathbf{r})] > 0. \quad (47)$$

The condition (47) imposes constraints on  $n_{bp}$  parameters that may be impractical for the actual implementation. However, we can simplify (47) by observing that it represents a half-space in  $n_{bp}$ -dimensional parameter space and thus by the adequately defined rotation we can map the parameter space  $\{c_{e,1}, \dots, c_{e,n_b}\}$  into a new one  $\{c'_{e,1}, \dots, c'_{e,n_b}\}$  where the constraint (47) transforms into  $c'_{e,i} > 0$  for an arbitrary  $i$  (determined by the rotation mapping).

There are two different types of active parameters in the model (40): spatial, which models the spatial dependence of the contractile stress, and temporal, which models the temporal pattern of the contraction. The spatial dependence is determined by the fiber angles which change continuously from the endocardium to epicardium and thus are not known. However, the number of time parameters can be reduced using equation (9). The length of systole (diastole) and time to peak-tension can be determined approximately (but with sufficient accuracy) from the pressure measurements. The relaxation time is deformation (strain) dependent parameter which cannot be determined.

## 5.2. Statistical Model

To obtain a statistical model, we use the following assumptions: the MR images are taken at time points  $\{t_k = k\Delta t, 1 \leq k \leq n\}$ , where  $\Delta t$  is the time interval between two consecutive images,  $n$  is the number of images per heart cycle, the nodal displacement vectors  $\mathbf{d}_k = \mathbf{d}(t_k)$  are measured exactly from each image, and the ventricular pressures  $p_k^{LV} = p^{LV}(t_k)$  and  $p_k^{RV} = p^{RV}(t_k)$  are measured during image acquisition. Using these measurements we wish to estimate the mechanical properties  $\boldsymbol{\theta} = [\boldsymbol{\theta}_a^T, \boldsymbol{\theta}_p^T]^T$ .

Before applying estimation techniques, we need to solve the differential equation (33) describing the heart motion. In the following, we derive the exact and an approximate (but computationally efficient) solutions. We obtain the approximate solution using a finite-difference approximation for the second-order derivatives and applying Fourier series approximation.

### Finite-Difference Approximation

Next, using models (43) and (40) we define

$$A(\boldsymbol{\theta}, t) = \int_S (\mathcal{D}\Phi)^T \tilde{E}(\boldsymbol{\theta}, \mathbf{r}) (\mathcal{D}\Phi) d\mathbf{r} + \int_{l_{epi}} \kappa \Phi^T \mathbf{n}_{epi} \mathbf{n}_{epi}^T \Phi d_l, \quad (48)$$

where by  $\tilde{E}(\boldsymbol{\theta}, \mathbf{r})$  we denote that stiffness related matrix is modeled using the parametric model (43). Next let  $A_k(\boldsymbol{\theta}) = A(\boldsymbol{\theta}, t_k)$  and  $M_k = M(t_k)$ . Then, using a discrete, second order derivative

$$\left. \frac{\partial^2 \mathbf{d}(t)}{\partial t^2} \right|_{t=t_k} = \frac{1}{\Delta t^2} (\mathbf{d}_{k+1} - 2\mathbf{d}_k + \mathbf{d}_{k-1}), \quad (49)$$

we approximate the differential equation (33) The differential equation (33) becomes

$$\frac{M_k}{\Delta t^2} \mathbf{d}_{k+1} + \left( A_k(\boldsymbol{\theta}) - \frac{2M_k}{\Delta t^2} \right) \mathbf{d}_k + \frac{M_k}{\Delta t^2} \mathbf{d}_{k-1} = \mathbf{f}_k. \quad (50)$$

Then, we lump the nodal displacements into one vector  $\mathbf{d} = [\mathbf{d}_1^T, \dots, \mathbf{d}_n^T]^T$ , and similarly the load vector  $\mathbf{f} = [\mathbf{f}_1^T, \dots, \mathbf{f}_n^T]^T$  where  $\mathbf{f}_k = \mathbf{f}(t_k)$ . Then equation (50) becomes

$$\mathbf{f} = [\rho \bar{M} T + \bar{A}(\boldsymbol{\theta})] \mathbf{d}, \quad (51)$$

where  $\bar{M} = \text{bdiag}(M_1, \dots, M_n)$ ,  $\bar{A}(\boldsymbol{\theta}) = \text{bdiag}[A_1(\boldsymbol{\theta}), \dots, A_n(\boldsymbol{\theta})]$ , and  $T$  is a Toeplitz matrix given by

$$[T_{i,j}] = \begin{cases} -2/(\Delta t)^2 & \text{for } i = j \\ 1/(\Delta t)^2 & \text{for } |i - j| = 1 \\ 0 & \text{elsewhere.} \end{cases} \quad (52)$$

In the ensuing discussion we will use model (51) because of its computational simplicity although the virtual displacement equation can be solved using more complex methods such as Fourier Series Approximation.

### 5.3. Non-Linear Optimization

Using (51) we approximate the measurement model as

$$\mathbf{y}_k \approx \mathbf{f}_k(\boldsymbol{\theta}) + \mathbf{e}_k, \quad (53)$$

where

$$\mathbf{f}_k(\boldsymbol{\theta}) = \frac{M_k}{\Delta t^2} \mathbf{d}_{k+1} + \left( A_k(\boldsymbol{\theta}) - \frac{2M_k}{\Delta t^2} \right) \mathbf{d}_k + \frac{M_k}{\Delta t^2} \mathbf{d}_{k-1} \quad (54)$$

and  $\mathbf{y}_k$  are the load vectors computed from pressure and displacement measurements,  $\mathbf{f}_k(\boldsymbol{\theta})$  are the model predicted load vectors corresponding to the material parameters  $\boldsymbol{\theta}$ , and  $\mathbf{e}_k$  is the vector of error residuals.

We seek a vector of material parameters  $\hat{\boldsymbol{\theta}}$  that minimizes the objective function

$$c(\boldsymbol{\theta}) = \sum_{k=1}^n \|\mathbf{y}_k - \mathbf{f}_k(\boldsymbol{\theta})\|^2. \quad (55)$$

Because the material parameters are nonlinear variables contained implicitly in the FE stiffness matrix, the minimization of (55), and thus the solution of the parameter-estimation problem, requires a nonlinear optimization algorithm. Following the approach of [21], we choose the gradient search algorithm direction to maximize the first order part of  $c(\boldsymbol{\theta})$ , keeping the length of direction search vector fixed, see [21]. The details of our implementation are given in [22].

### 5.4. Estimating Residual Stress

To account for the residual strain  $\boldsymbol{\epsilon}_0(\mathbf{r}, t)$ , we first modify (6) by subtracting  $\boldsymbol{\epsilon}_0(\mathbf{r}, t)$  from the total strain  $\boldsymbol{\epsilon}(\mathbf{r}, t)$  i.e.

$$\begin{aligned} \boldsymbol{\sigma}^P(\mathbf{r}, t) &= E(\mathbf{r}, t)[\boldsymbol{\epsilon}(\mathbf{r}, t) - \boldsymbol{\epsilon}_0(\mathbf{r})] \\ &= E(\mathbf{r}, t)\boldsymbol{\epsilon}(\mathbf{r}, t) - \boldsymbol{\sigma}_0^P(\mathbf{r}), \end{aligned} \quad (56)$$

where  $\boldsymbol{\sigma}_0^P(\mathbf{r}, t)$  represents the residual stress. Observe that time variations of residual stress (strain) are due to heartwall deformation only i.e. they are *a priori* known. Next we

Next we compute the change in the work of internal forces  $w_i$  due to residual stress

$$\begin{aligned} \Delta w_i &= \int_{S(t)} (\mathcal{D}\delta v)^T \boldsymbol{\sigma}_0(\mathbf{r}, t) d\mathbf{r} \\ &= \mathbf{d}_{\delta v}^T \int_{S(t)} (\mathcal{D}\Phi(\mathbf{r}, t))^T \boldsymbol{\sigma}_0(\mathbf{r}, t) d\mathbf{r}. \end{aligned} \quad (57)$$

To estimate the residual stress we approximate  $\boldsymbol{\sigma}_0(\mathbf{r}, t)$  using a set of *a priori* known spatial basis functions and unknown coefficients, i.e. we model

$$\boldsymbol{\sigma}_0(\mathbf{r}) = W(\mathbf{r}, t)\boldsymbol{\omega} \quad (58)$$

where  $W(\mathbf{r}, t)$  is the spatial interpolation matrix and  $\boldsymbol{\omega}$  are the unknown coefficients. Recall that the time variations are due to heartwall deformation. Therefore, we only need to construct spatial basis functions for the reference state and then map them to different time points (according to heart motion).

The statistical model (51) then becomes

$$\mathbf{f} = [\rho \bar{M}T + \bar{A}(\boldsymbol{\theta})] \mathbf{d} + W\boldsymbol{\omega} \quad (59)$$

where

$$W = \begin{bmatrix} W(\mathbf{r}, t_1) \\ W(\mathbf{r}, t_2) \\ \vdots \\ W(\mathbf{r}, t_m) \end{bmatrix}. \quad (60)$$

### 5.5. Confidence Region

In this section we assess the estimator's performance by determining confidence regions for the parameter estimates. Confidence region is a range of parameter values containing the true values of the unknown parameters with a certain probability (see e.g. [23]). We assume that the error residuals arise from a zero-mean Gaussian distribution with unknown variance  $\sigma^2$ .

In the case of linear regression the confidence region can be based on a jointly sufficient set of statistics. On the other hand, in the non-linear case such a set is not available, in general. However, the exact confidence region can be constructed in the following way. Let  $\mathbf{y} = [\mathbf{y}_1^T, \dots, \mathbf{y}_n^T]^T$  and similarly  $\mathbf{e} = [\mathbf{e}_1^T, \dots, \mathbf{e}_n^T]^T$ . Then we construct the confidence region by taking any decomposition of the sum of squares  $\mathbf{e}^T \mathbf{e}$  into two quadratic forms  $\text{reg}(\mathbf{e})$  distributed as chi-square with  $n_\theta = \dim(\boldsymbol{\theta})$  of freedom and  $\text{res}(\mathbf{e})$  distributed as chi-square with  $n_y - n_\theta$  degrees of freedom where  $n_y = \dim(\mathbf{y})$ . These forms will be, by Cochran's theorem [23], independently distributed as  $\sigma^2 \chi^2$  with  $n_\theta$  and  $n_y - n_\theta$  degrees of freedom respectively. Therefore, the statement

$$\frac{\text{reg}(\mathbf{y} - \mathbf{f}(\boldsymbol{\theta}))}{\text{res}(\mathbf{y} - \mathbf{f}(\boldsymbol{\theta}))} \leq \frac{n_\theta}{n_y - n_\theta} F(\alpha, n_\theta, n_y - n_\theta) \quad (61)$$

provides an exact  $\alpha$  confidence region for  $\boldsymbol{\theta}$ , i.e. the region in parameter space which contains the true value of  $\boldsymbol{\theta}$  with probability  $\alpha$  [23]. The question now arises as to which decomposition should be chosen. It has been shown [24] that for essentially linear models, i.e. when

$$\mathbf{f}_k(\boldsymbol{\theta}) = \sum_{i=1}^{n_\theta} v_i(\boldsymbol{\theta}) U_{ki} \quad (62)$$

where  $v_i(\boldsymbol{\theta})$  are continuous functions of  $\boldsymbol{\theta}$  and  $U_{ki}$  are entries of matrix  $U$  which has rank  $n_\theta$  and is independent of  $\boldsymbol{\theta}$ . Whereas in general such a representation is not available, it is usually possible to approximate  $\mathbf{f}_k(\boldsymbol{\theta})$  as  $n_\theta$ -term linear forms of the parameter functions  $v_i(\boldsymbol{\theta})$ .

To develop a method of constructing an essentially linear approximation we use a Lagrangian approximation

$$\mathbf{f}_{\text{lag}}(\boldsymbol{\theta}) = \sum_{i=1}^{n_\theta} U_{ki} \mathbf{f}_k(\boldsymbol{\theta}) \quad (63)$$

where

$$U_{ki} = \frac{\prod_{j=1}^{n_\theta} (k - j)}{\prod_{j=1}^{n_\theta} (i - j)}. \quad (64)$$

Using the approximation (63) we choose the quadratic forms

$$\begin{aligned} \text{reg}(\mathbf{e}) &= (U^T \mathbf{e})^T (U^T U)^{-1} (U^T \mathbf{e}) \\ \text{res}(\mathbf{e}) &= \mathbf{e}^T \mathbf{e} - \text{reg}(\mathbf{e}) \end{aligned}$$

for the construction of an exact  $\alpha$ -confidence region. Although the accuracy of the approximation (63) in no way affects the exactness the confidence region, any failure in the accuracy of (63) will result in larger departures of the boundary of the confidence region from a contour of the constant likelihood given by

$$\mathbf{e}^T \mathbf{e} = \text{const}. \quad (65)$$

Observe that any transformation of  $U$  by a non-singular  $n_\theta \times n_\theta$  matrix  $A$  with constant coefficients will yield the same form for  $\text{reg}(\mathbf{e})$ . Therefore the Lagrangian approximation is only one of several representations which yield the same confidence region.

### 6. Numerical Examples

In this section we demonstrate the applicability of our results by numerical examples.

*Example 1*

We first conduct a numerical study using computer-synthesized data. The purpose of this study is to examine the effects of the measurement noise on the estimated mechanical properties and to verify the theoretical analysis. The example considers the heart’s cross-sectional plane obtained from an early diastolic MR image (see Figure 1).

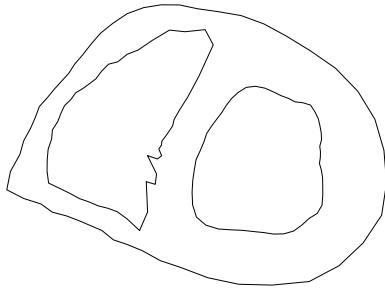


**Figure 1:** Heart’s cross-section.



**Figure 2:** Elasticity modulus (simulated).

We model the passive properties using  $\{1, x, y, xy, x^2, y^2\}$  as basis functions for the elasticity modulus, see (45). Similarly, for the active properties, we use  $\{1, \cos x, \cos y, \sin x, \sin y, \cos(xy), \sin(xy)\}$  for generating the active stress (40). We select the later basis functions as appropriate for modeling cross-sectional variations of the active stress due to changes in the fiber elevation and azimuth angles. We assume that the Poisson ratio is constant over the heart’s cross-section and since the heart is nearly an incompressible material we set the Poisson ratio to  $\epsilon = 0.45$  (see [6]) and density  $\rho = 1.06\text{kg/m}^3$ . Using these values, in Figures 2-3 we illustrate the simulated mechanical properties, elasticity modulus and active stresses.

We adopt the numerical values describing the time-dependent activation model (8) from [16]:  $t_0 = 0.1\text{s}$  and  $t_r = 0.4\text{s}$ . The heart periodic rate is set to  $t_c = 0.83\text{s}$ , corresponding to a heart rate of 72 beats per minute. The pressure measurements were simulated using the empirical model [25]

$$p(t) = \begin{cases} p_{ED} + \frac{p_{Peak} - p_{ED}}{2} \left(1 - \cos\pi \frac{t}{t_{Peak}}\right) & \text{for } 0 \leq t \leq t_{Peak}, \\ p_{ES} + p_{Peak} - p_{ES} \{1 - \exp[-\mu(t_{ES} - t)]\} & \text{for } t_{Peak} \leq t \leq t_{ES} \end{cases}, \tag{66}$$

where  $p_{ED} = 5\text{mm[Hg]}$  is the end-diastolic pressure,  $p_{Peak} = 160\text{mm[Hg]}$  is peak pressure,  $t_{Peak} = 0.35\text{s}$  is time-to-peak pressure,  $p_{ES} = 35\text{mm[Hg]}$  is end-systolic pressure,  $a$  is a constant, and  $t_{ES} = 0.45\text{s}$  is time-to-end-systolic pressure. Figures 4 and 5 show the ventricular pressures as a function of time obtained from (66).

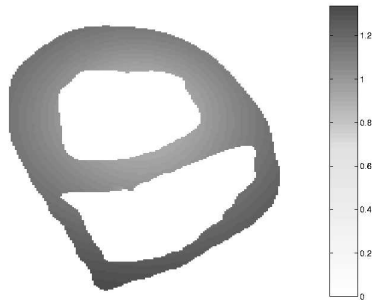


**Figure 3:** Active stress (simulated).

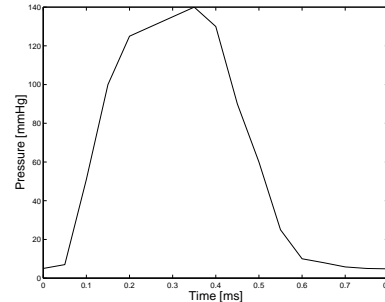


**Figure 4:** Left-ventricular pressure, empirical model.

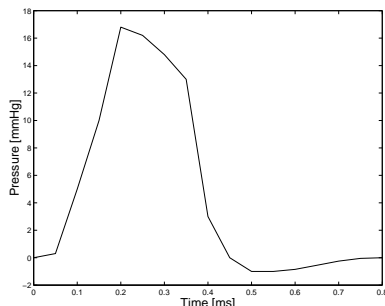


**Figure 5:** Right-ventricular pressure, empirical model.



**Figure 6:** Elasticity modulus (estimated, SNR=20dB).

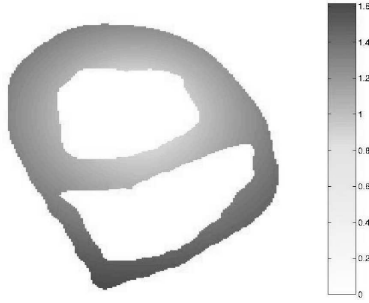


**Figure 7:** Active stress (estimated, SNR=20dB).



**Figure 8:** Elasticity modulus (estimated, SNR=5dB).

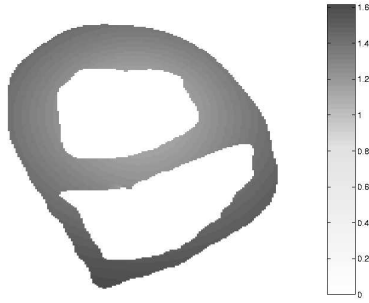


**Figure 9:** Active stress (estimated, SNR=5dB).



**Figure 10:** Elasticity modulus (estimated, hybrid data).

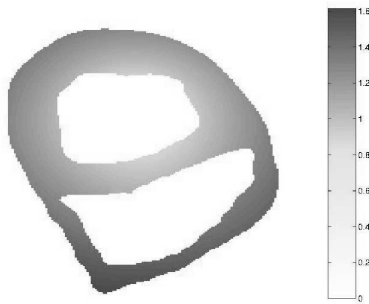


**Figure 11:** Active stress (estimated, hybrid data).



**Figure 12:** Elasticity modulus (estimated, hybrid data).

The time increment (time interval between two consecutive images)  $\Delta t$  was set to 0.02s. We adopt the spring constant  $k = 135\text{N/m}^3$  from [6] to model the pericardial effects on the heart's motion.

To account for the possible errors, we add Gaussian noise to the pressure measurements. We define the signal-to-noise ratio (SNR) as the ratio of signal (pressure measurements) power to noise variance. We test the sensitivity of the algorithm for two cases: SNR= 20dB and 5dB. In both cases we estimate the mechanical properties using the numerical optimization technique presented in Section 5.3

Figures 6 and 7 illustrate the estimated mechanical properties for high SNR (20dB). To assess the accuracy of the proposed technique we performed the non-linear optimization (55) using different initial guesses. Convergence of the parameter estimates was judged to have occurred when both active and passive parameters changed by less than 1% between successive iterations or the value of the objective function changed by less than 0.01% between two iterations. On a regional basis the root-mean-squared (RMS) error between the estimated and the actual mechanical properties varied from 0.03 to 0.05. Figures 8 and 9 illustrate the estimated mechanical properties for low SNR=5dB. In this case, the parameter estimates of the active properties varied by as much as 30%. The passive properties estimates varied from 10% to 18%. Although these variations may seem high they are still on the order of the added noise ( $\pm 30\%$ ). The results of this study support the conclusion that the proposed myocardial material parameter estimation is not overly sensitive to uncertainties in the measurements.

#### Example 2

We tested the performance of our method *in vivo* on a sequence of MR images kindly provided to us by GE Medical Systems, Milwaukee, WI. The purpose of this experiment is to demonstrate that the method performs effectively with *in vivo* hybrid data (real MR images and simulated pressure measurements) and is useful at SNR and artifact levels that can be expected in clinical studies.

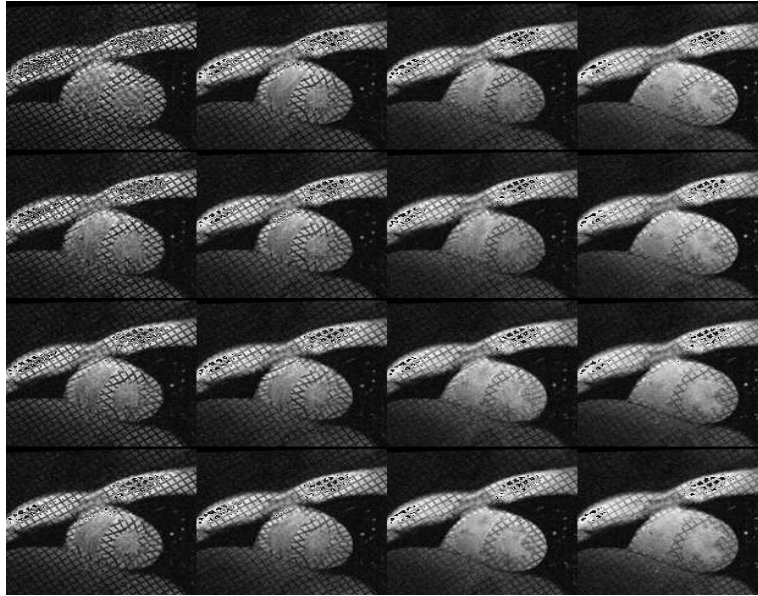


**Figure 13:** Tagged MRI sequence of the cross-sectional plane of the heart beginning at early systole and ending at late diastole.

The MRI sequence consisted of 21 short-axis (trans-axial) mid-ventricular images obtained with 20ms time intervals. The images were reconstructed to the  $32\text{cm} \times 32\text{cm}$  field-of-view (FOV). The dimensions of the acquisition matrix were  $256 \times 256$  pixels with effective resolution of 1.25mm in-plane.

The displacement field was obtained by tracking the tag points in the following way. We first displayed each image retaining the global Cartesian coordinate system established by the MR scanner. We selected manually seed points along the borders of each tag line. Then we constructed 6-order polynomial approximations (two for each tag line) for each set of the seed points. Using these approximations we obtained the intersection area for each pair of tag lines. Finally we computed a “true” location of each tag point as a weighted gravity center of the intersection area using pixel intensities as weighting coefficients.

We computed 2D in-plane strains for each of the 45 quadrilateral elements formed by the tag lines for the deformation throughout the heart cycle. Calculations were made for each element using the global Cartesian coordinate system established by the scanner.

Estimating the unknown mechanical properties  $\theta$  using the model (5.3) requires the knowledge of the intra-ventricular pressures. Since our sequence of MR images was acquired without simultaneous pressure measurements, we used synthetic pressure data generated using the model (66). We performed the non-linear optimization algorithm from Section 5.3 for a wide range of values for pressure parameters describing the (66). We selected those pressure parameters that give the minimal RMS error between the predicted and measured displacement of tag points. As a result, we obtained the following parameters for the left-ventricular pressure: the end-diastolic pressure 5mm[Hg], peak pressure 160mm[Hg], time-to-peak pressure 0.35s, end-systolic pressure 35mm[Hg], and time-to-end-systolic pressure 0.45s. Similarly for the right-ventricular pressure the end-diastolic pressure was 0mm[Hg], peak pressure 20mm[Hg], time-to-peak pressure 0.2s, end-systolic pressure 5mm[Hg], and time-to-end-systolic pressure 0.45s

As in the previous example, we set the Poisson’s ratio at 0.45 and performed the non-linear optimization on the remaining parameters. Figures 11 and 12 show the estimated mechanical properties for this scenario. We assessed the regional accuracy of our estimates by computing the 95% confidence region, see Table 1. The columns represent 12 vectors corresponding to the axes of the confidence region ellipsoid in the parameter space. The estimated vector of mechanical properties is  $\{3.2, 0.53, 4.59, 6.71, 1.32, 2.71, 0.12, 0.05, 3.11, 1.13, 2.13, 3.4, 0.78\}$ . In addition, we computed the differences between the strains predicted by the model and those measured using MR. Figure 12 shows graphically these differences for each individual measurement location. In general, there is not a uniform pattern that would suggest that the model predictions were most accurate for any particular small region.

Observe that our results indicate significant spatial variability of both stiffness and active stresses in the heart’s cross-section. Therefore, our globally defined spatial basis functions model should allow more accurate description of the mechanical properties.

95% Confidence region												
	1	2	3	4	5	6	7	8	9	10	11	12
$C_1^e$	-0.96	6.78	4.95	0.70	5.47	5.58	3.55	3.48	1.87	3.12	1.40	-0.83
$C_2^e$	-0.61	3.74	1.28	0.21	8.59	-1.51	0.87	4.94	-1.47	13.07	1.08	0.12
$C_3^e$	3.10	0.62	1.09	0.57	4.35	3.91	2.73	1.40	1.51	7.55	11.60	1.25
$C_4^e$	1.22	2.12	3.11	0.45	5.01	6.07	0.71	4.56	0.91	1.08	1.16	4.12
$C_5^e$	7.64	5.42	0.37	4.05	0.15	6.21	0.37	4.18	0.91	1.57	3.11	1.26
$C_6^e$	-8.82	4.17	3.56	-13.13	9.165	4.17	-2.81	9.44	8.07	5.17	3.11	-8.12
$C_7^e$	2.14	-3.56	7.13	2.10	5.35	4.16	-7.21	1.18	-3.19	7.10	6.11	-3.27
$C_8^e$	10.8	6.29	2.77	-2.26	-10.61	-7.13	-11.63	-1.95	8.11	0.06	-7.36	4.75
$C_9^e$	-6.42	-1.04	7.00	10.45	-3.53	-7.23	-5.92	8.31	-11.53	5.03	4.37	-2.92
$C_{10}^e$	2.56	-11.55	10.12	10.00	7.52	2.49	-1.32	0.60	4.35	-1.71	-4.73	8.64
$C_{11}^e$	-0.33	7.71	5.72	-2.15	-11.76	-5.47	10.36	-7.14	-2.89	-4.69	1.00	8.49
$C_{12}^e$	9.39	-1.32	-7.77	9.45	-8.67	-7.23	-0.82	3.13	7.96	-7.45	-8.37	2.25

Table 1. Confidence region (95%).

### 7. Conclusions

We have presented a method for estimating both active and passive properties of the *in vivo* heart. We derived a dynamic model for the mechanical activity of the heart by including inertial forces and time dependent activation model describing the contractile stress during systole. In addition, we proposed to improve the modeling accuracy using a non-homogeneous model for the mechanical properties. We modeled the non-homogeneity of these properties using a set of *a priori* known basis functions and unknown coefficients. We estimated these coefficients using a non-linear optimization algorithm which minimizes the error between the model-predicted and measured load vectors. Our method offers a potential for testing constitutive models of the *in vivo* whole heart, since it allows estimation of both active and passive properties.

Application of the finite element method for solving inverse problems requires a description of the ventricular geometry in a reference state. We selected tagged MRI for this study because of its excellent spatial and temporal resolution, the non-invasive character of this imaging technique, and most importantly, its ability to track the motion of particular points within the myocardium.

The results of the second numerical example suggest substantial spatial variability of both passive and active properties. Therefore, assuming constant properties over a single element may not provide sufficient accuracy for modeling spatial non-homogeneity. Our globally defined spatial basis functions model allows us to model these spatial variations of the mechanical properties more accurately and hence, gives better estimates of these properties.

Future work will include similar analysis with 3D model together with more complex models of active contraction and passive relaxation. The details of the heart’s mechanical behavior and other complexities inherent to 3D modeling of the heart *in vivo* can be added systematically to the model without altering the basic method of solving the inverse problem. Using 3D analysis we will resolve the problem of through-plane motion which ultimately affects the accuracy of mechanical property estimates. In addition, such analysis will include the out-of-plane component of strain, thus reducing the strain measurement error.

An effort should be made to examine the robustness of the proposed method with respect to certain random effects. Namely, due to the lengthy MRI acquisition time a substantial geometric variability can occur over time leading to blurs in the MR images. Therefore, the tag point locations should be considered as random variables. Since tag points are the FE mesh nodes, an adequate stochastic analysis of this effect can be performed. In addition, we will examine random effects due to pressure variability and consequently uncertainty in the mean value of the observer pressure change during heart cycle.

Finally, to confirm the applicability of the proposed method in a clinical environment, it would be useful to compare the estimated mechanical properties of healthy and diseased subjects.

### Acknowledgment

We thank Dr. Jason Polzin, GE Medical Systems, Milwaukee, WI, for providing us the sequence of MR images.

[1] Bers, D. M. (2001), *Excitation Contraction Coupling and Cardiac Contractile Force*, Kluwer Academic, Dordrecht, Netherlands.  
 [2] Pogwizd, S. M. Schlotthauer, K. Li, L. Yuan, W. and Bers, D.M., (2001) “Arrhythmogenesis and contractile dysfunction in heart failure: roles of sodiumcalcium exchange, inward rectifier potassium current and residual -adrenergic responsiveness,” *Circ. Res.*, vol. 88, pp. 1159-1167.

- [3] Rankin, J. S., Arentzen C. E., Ring W. S., Edvards C. H., McHale P. A., and Anderson R. W. (1980), "The diastolic mechanical properties of the intact left ventricle," in *Federation Proc.*, vol. 39, pp. 141-147.
- [4] Hess, O. M., Bhargava, V., Ross, J., and Shabetai, R. (1983), "The role of the pericardium in interaction between the cardiac chambers," *Am. Heart J.*, vol. 106, pp. 1377-1383.
- [5] Biot, M. A. (1948), *Mechanics of Incremental Deformations*, John Wiley & Sons, New York.
- [6] Moulton, M. J., Creswell, L. L., Actis, R. L., Myers, K. W., Vannier, M. W., Szabo, B. A., and Pasque, M. K. (1995), "An inverse approach to determining myocardial material properties," *Journal of Biomechanics*, Vol. 28, pp. 935-947..
- [7] Axel, L., and Dougherty, L.(1989), "Heart wall motion - improved method of spatial modulation of magnetization for MR imaging," *Radiology*, vol. 172, no. 8, pp. 349-350.
- [8] Huyghe, J. M., Arts, T., van Campen, D. H., and Reneman R. S. (1992). "Porous medium finite element model of the beating left ventricle," *American Journal of Physiology*, vol. 26, pp. H1256-1267.
- [9] Fozzard, H. A. and Solaro, R. J. (2001) *Handbook of Physiology*, Oxford Univ. Press, New York.
- [10] Fung, Y. C. (1987), *Biomechanics*, Springer-Verlag, New York.
- [11] Fung, Y. C. (1984), *Biodynamics*, Springer-Verlag, New York.
- [12] Streeter, Jr. D. D., Powers, W.E., Ross, M.A., and Torrent-Guasp, F. (1978), "Three-dimensional fiber orientation in the mammalian left ventricular wall," in J. Baan, A. Noordergraaf, and J. Raines (eds), *Cardiovascular System Dynamics*, pp. 73-84, MIT Press, Cambridge, MA.
- [13] Nielsen, P.M.F., Le Grice, I. J., Smaill, B. H., and Hunter, P. J. (1991), "Mathematical model of geometry and fibrous structure of the heart," *American Journal of Physiology*, vol. 26, pp. H1365-H1378.
- [14] Hunter, P.J., Smaill, B.H., Nielsen, P.M.F., and Le Grice, I.J. (1997), "A mathematical model of cardiac anatomy," *Computational Biology of the Heart*, eds. A. V. Panfilov and A. V. Holden, John Wiley & Sons, New York.
- [15] Moss, R. L. and Buck, S. H. (2001), in *Handbook of Physiology* (eds Page, E., Fozzard, H. A., and Solaro, R. J.) pp. 420454 (Oxford Univ. Press, New York.
- [16] Guccione, J. M., and McCulloch, A. D. (1993), "Mechanics of active contraction in cardiac muscle," *ASME J. Biomech. Engng.*, vol. 115, pp. 82-90.
- [17] Guccione, J.M., McCulloch, A.D., and Waldman, K.L. (1993), "Passive material properties of intact ventricular myocardium determined from a cylindrical model," *ASME Journal of Biomechanical Engineering*, vol. 113, pp. 42-55,
- [18] Zienkiewicz, O.C., and Morgan, K. (1983), *Finite Elements and Approximation*, John Wiley & Sons, New York.
- [19] Szabo, B., and Babuska, I., (1991). *Finite Element Analysis*, John Wiley & Sons, New York.
- [20] Gordon, W. J. (1971), "Blending function methods of bivariate and multivariate interpolation and approximation," *SIAM J. Numer. Anal.*, vol. 8, pp. 158-177.
- [21] Crocket, J. B., and Chernoff, H. (1993), "Gradient methods of maximization," *Pacific Journal of Mathematics*, vol. 5, pp. 33-50.
- [22] A. Jeremic and A. Nehorai, "Estimating mechanical properties of the heart using dynamic modeling and magnetic resonance imaging," Dept. Elect. Eng. Comput. Sci., Univ. Illinois at Chicago, Rep. UIC-EECS-00-11, Nov. 2000.
- [23] Rao, C. R. (1973), *Linear Statistical Inference and Its Applications*, John Wiley & Sons, New York, 2nd ed.
- [24] Hartley, B. O. , "Confidence interval estimation in non-linear regression," Program 360, Applied Mathematics Department SRRC-RR-62-28, Sperry-Rand Research Center.
- [25] Waldman, L. K., Nosan, D. Villareal, F., and Covell, J. W. (1988), "Relation between transmural deformation and local myofiber direction in canine left ventricle," *Circ. Res.*, vol. 63, pp. 550-562.